

# Supplementary Information for "Understanding biases and changes in future European extreme rainfall using dynamical flow precursors"

jcfdorrington

March 2025

## 0.1 Supplementary figures

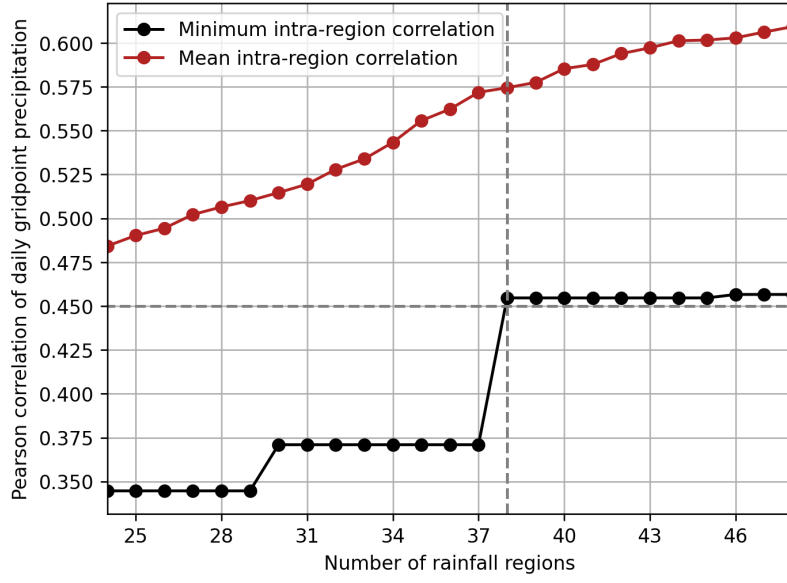


Figure 1: The minimum and mean correlation of ERA5-land daily precipitation between any two gridpoints assigned to the same region over the period 1979-2023, as a function of the number of regions. Regions were defined using an agglomerative clustering of the precipitation cross-correlation matrix, as described in the main text. The dashed horizontal line marks the 0.45 minimum correlation used as a heuristic threshold to define region number. The vertical dashed line marks correlation values for the 38 region configuration used in the main text.

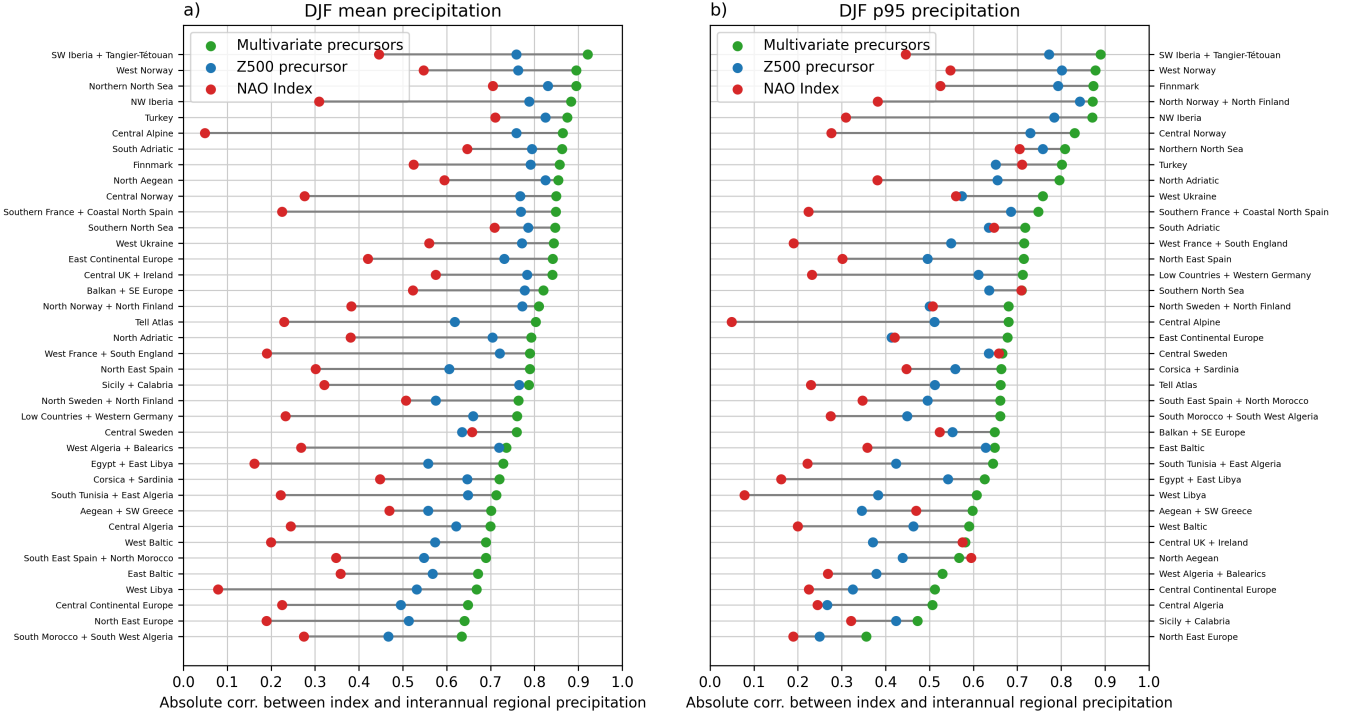


Figure 2: Positively oriented pearson correlations are shown between DJF mean values of different dynamical indices and DJF mean (a) / DJF 95th percentile (b) seasonal precipitation totals for each region over the period 1979-2023. The NAO index is included for reference, defined as the first cosine-latitude weighted principal component of Z500 over [80W-40E,30-85N], and is the same index for every region. The Z500 precursor is defined as in the main text, and is distinct for each region. ‘Multivariate precursors’ are the first principal component of U850, V850 and Z500 precursor indices, as used to define  $S$  in the main text. Regions have been ordered by multivariate precursor correlation, and are ordered differently in each panel. Z500 precursors show stronger and more consistent correlations with both mean and heavy precipitation than the NAO index in almost every region. Multivariate precursors perform better still, even though the U850, V850 and Z500 precursors are often closely correlated.

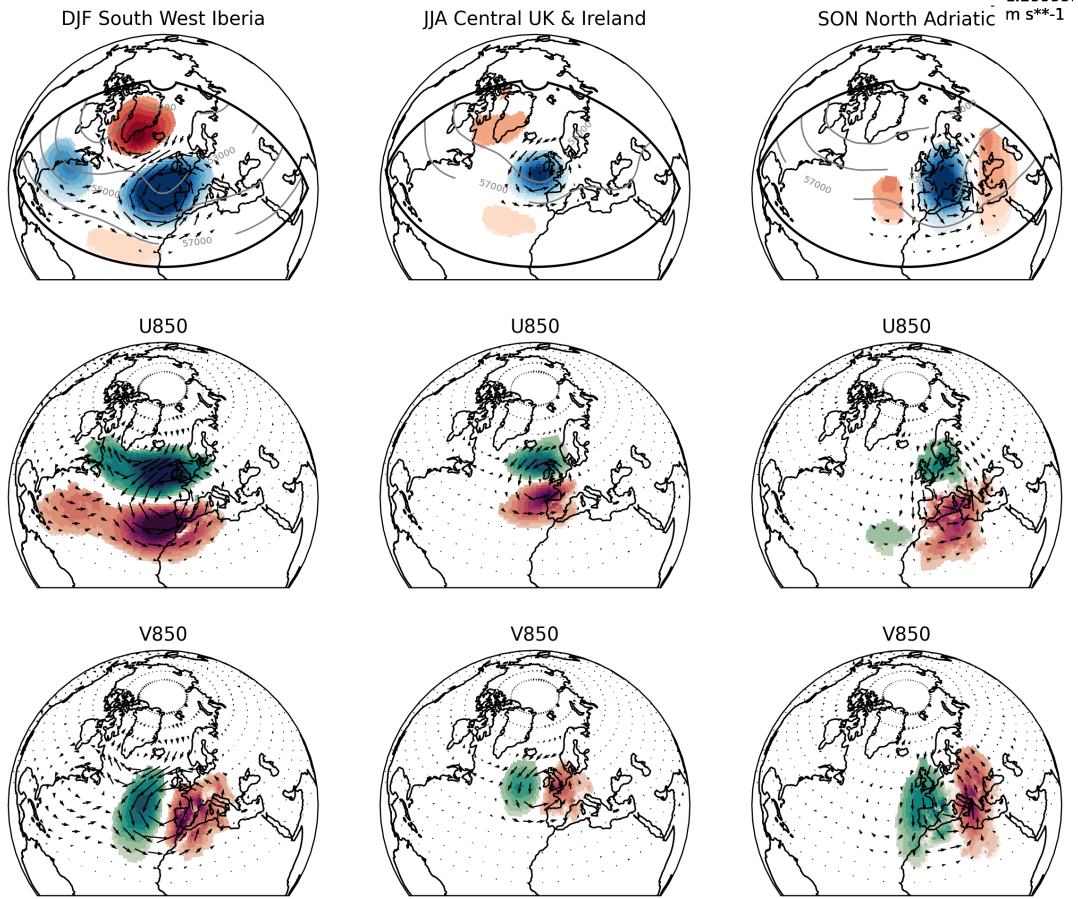


Figure 3: ERA5 precursor patterns for the three region-seasons discussed individually in the main text, and as in Figure 4 but with more detail. Row 1 shows 500 hPa geopotential height (Z500) precursor patterns in shading, with grey lines marking selected full field contours of geopotential. Row 2 shows 850 hPa zonal wind (U850) precursors in shading, and row 3 shows 850 hPa meridional wind (V850) precursors in shading. In each panel shaded anomalies are on an arbitrary standardised scale, with red colors indicating positive anomalies. Arrows in all panels show 850 hPa wind anomalies, in Row 1 only for gridpoints where a U850 and/or V850 precursor is present.



	95th percentile threshold (mm/day)			
Region	DJF	MAM	JJA	SON
Turkey	12.4	8.0	2.6	8.9
Aegean + SW Greece	9.1	5.7	<i>2.1</i>	7.4
North Norway + North Finland	13.0	9.3	9.8	12.2
Central Norway	13.1	9.6	11.5	12.5
Finnmark	6.3	6.1	10.2	8.3
West Ukraine	6.2	8.0	11.2	8.4
East Continental Europe	7.2	8.1	9.8	9.4
Central Continental Europe	7.9	8.3	10.7	8.8
North East Europe	5.3	6.0	8.5	6.9
North Adriatic	12.8	11.1	8.6	16.4
Central Alpine	12.5	12.6	12.5	16.4
Northern North Sea	16.3	10.5	10.3	14.8
West Norway	25.8	16.9	15.6	24.0
West Libya	<i>2.2</i>	<i>1.2</i>	<i>0.1</i>	<i>1.4</i>
Egypt + East Libya	<i>2.2</i>	<i>1.2</i>	<i>0.1</i>	<i>1.0</i>
North Sweden + North Finland	4.8	5.0	8.5	6.7
Central Sweden	6.6	6.5	9.8	8.6
East Baltic	5.9	5.3	8.3	7.3
West Baltic	5.7	5.4	7.7	6.2
Corsica + Sardinia	7.3	7.2	<i>2.3</i>	7.9
Tell Atlas	7.4	6.6	<i>1.4</i>	6.3
Sicily + Calabria	9.5	7.1	2.7	9.2
South Tunisia + East Algeria	<i>2.2</i>	<i>2.0</i>	<i>0.5</i>	<i>1.9</i>
Central Algeria	<i>1.5</i>	<i>1.4</i>	<i>0.2</i>	<i>1.6</i>
West Algeria + Balearics	4.1	4.3	<i>0.9</i>	4.0
South Morocco + South West Algeria	3.4	2.6	<i>0.6</i>	2.9
South East Spain + North Morocco	6.9	6.4	<i>2.0</i>	6.9
North East Spain	6.5	7.4	5.6	8.4
Southern France + Coastal North Spain	10.0	10.3	9.1	12.5
NW Iberia	15.7	11.6	5.6	15.0
SW Iberia + Tangier-Tétouan	12.0	8.4	<i>1.7</i>	11.4
West France + South England	9.3	7.8	7.9	9.2
Low Countries + Western Germany	9.1	7.5	8.3	8.9
Central UK + Ireland	8.6	7.0	7.5	8.6
Southern North Sea	9.2	7.7	9.2	10.5
Balkan + SE Europe	6.7	8.0	8.4	8.3
South Adriatic	13.6	10.8	6.2	13.8
North Aegean	11.5	8.3	5.0	11.2

Table 1: 95th daily area-averaged precipitation thresholds used to define heavy precipitation for each region. Thresholds below 2.5 mm/day are marked in italics, and excluded from tendency and bias plots.

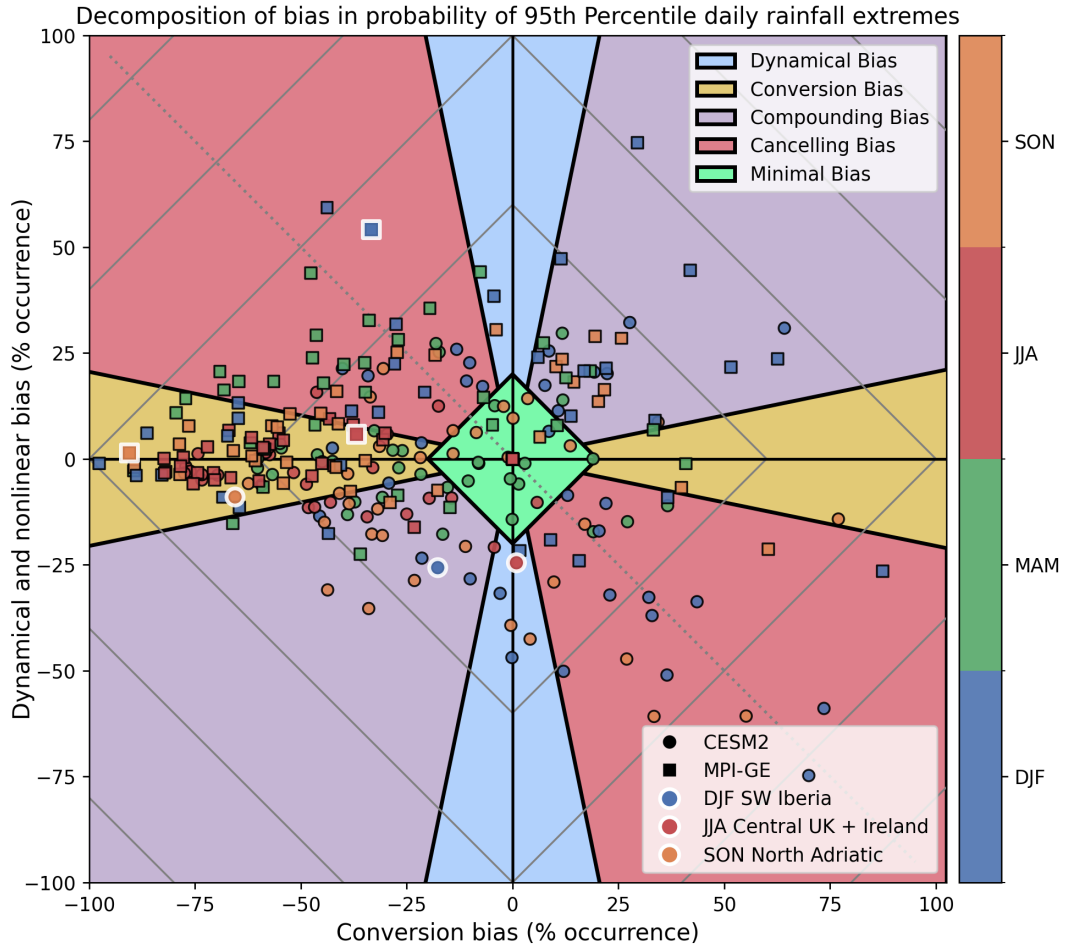


Figure 4: Heavy precipitation biases visualised in a bias space as described in the main text. Ensemble mean results are shown for every region-season excluding cases where the heavy precipitation threshold is below 2.5mm/day. The three cases discussed in the main text are distinguished with a white border.

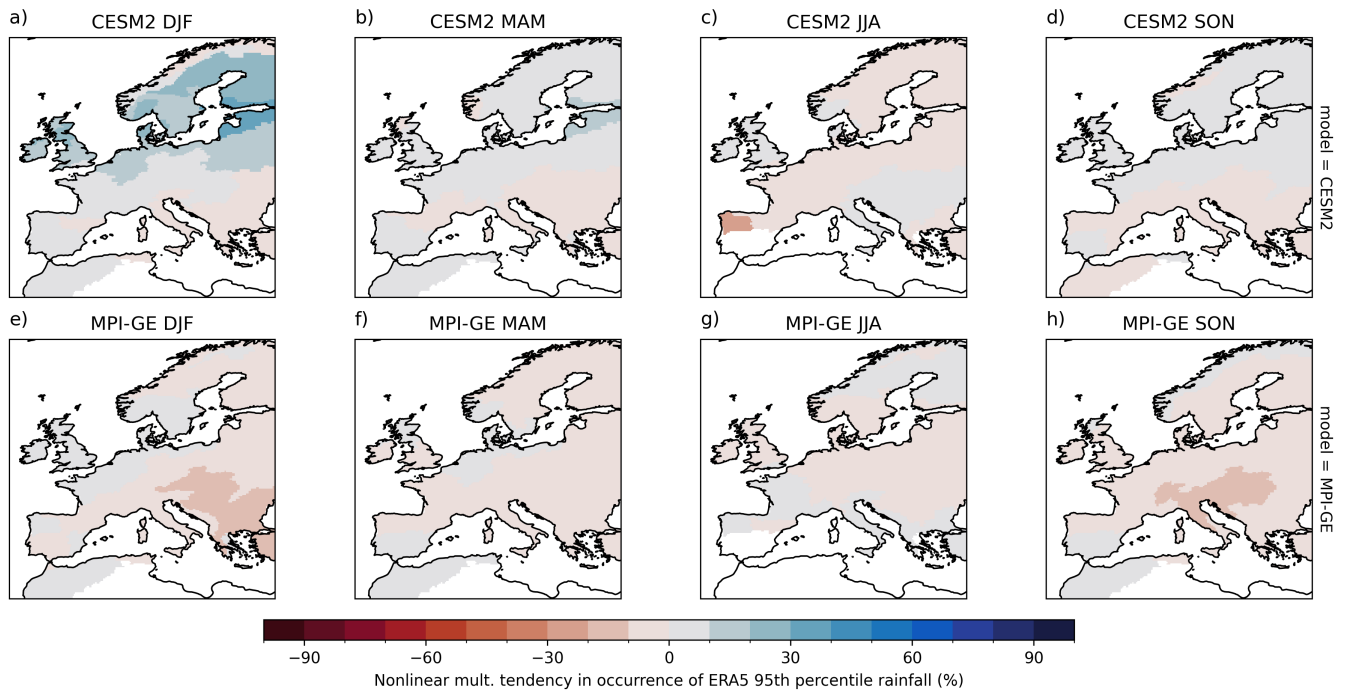


Figure 5: Ensemble mean relative tendencies (2060-2100, SSP3-7.0) in heavy precipitation occurrence attributable to nonlinear interactions of dynamical and conversion tendencies. Results are not shown for region-seasons where the historical heavy precipitation threshold is less than 2.5mm/day

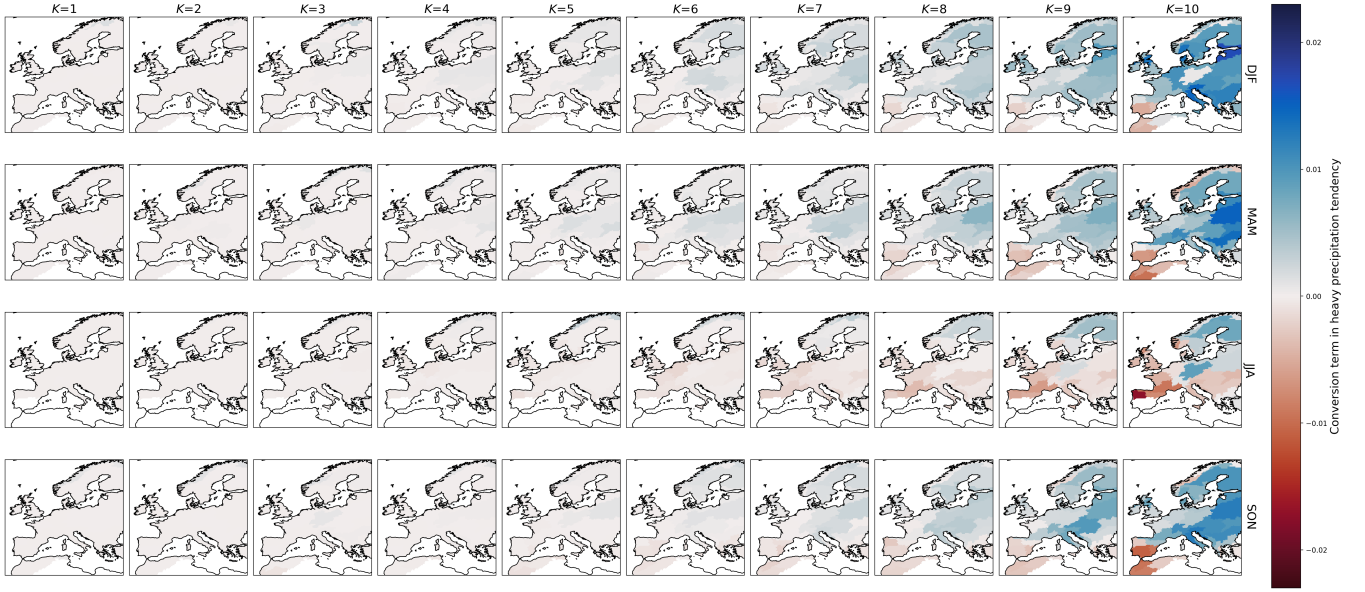


Figure 6: Ensemble mean conversion tendencies decomposed by synoptic bin for CESM2 for each season. If new dynamical processes were causing heavy precipitation in the future simulations this would be visible as increased conversion rates for weak or negative precursors. Instead the majority of conversion signal is combined to bins  $K=[8,9,10]$ .

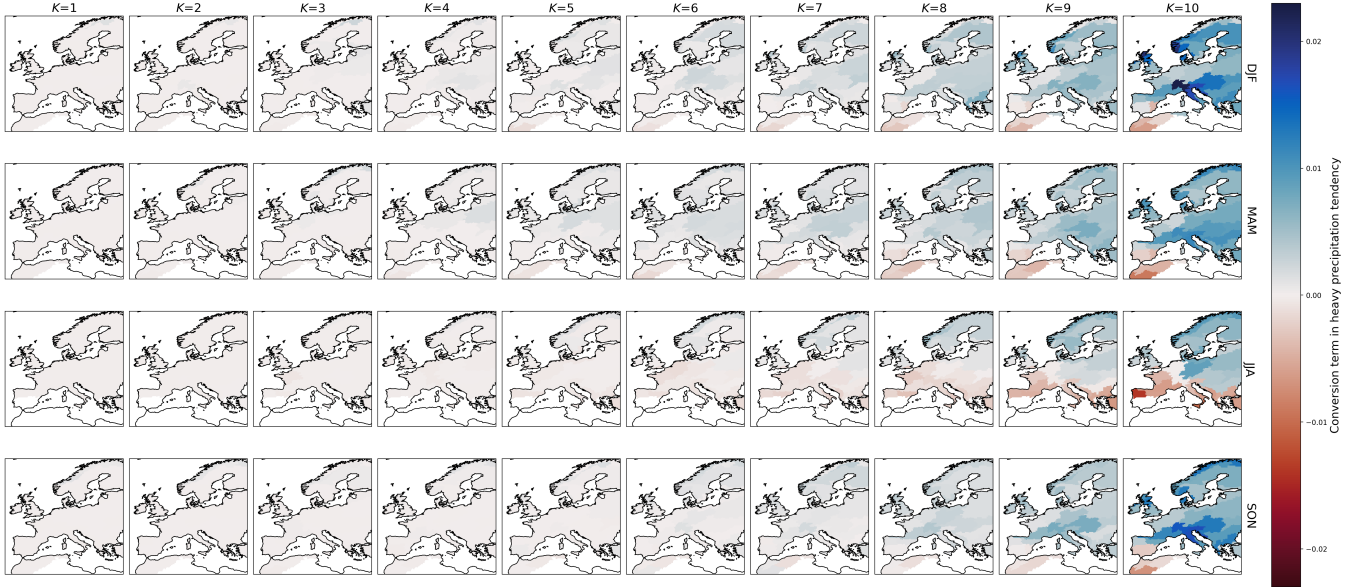


Figure 7: Ensemble mean conversion tendencies decomposed by synoptic bin for MPI-GE for each season. If new dynamical processes were causing heavy precipitation in the future simulations this would be visible as increased conversion rates for weak or negative precursors. Instead the majority of conversion signal is combined to bins  $K=[8,9,10]$ .

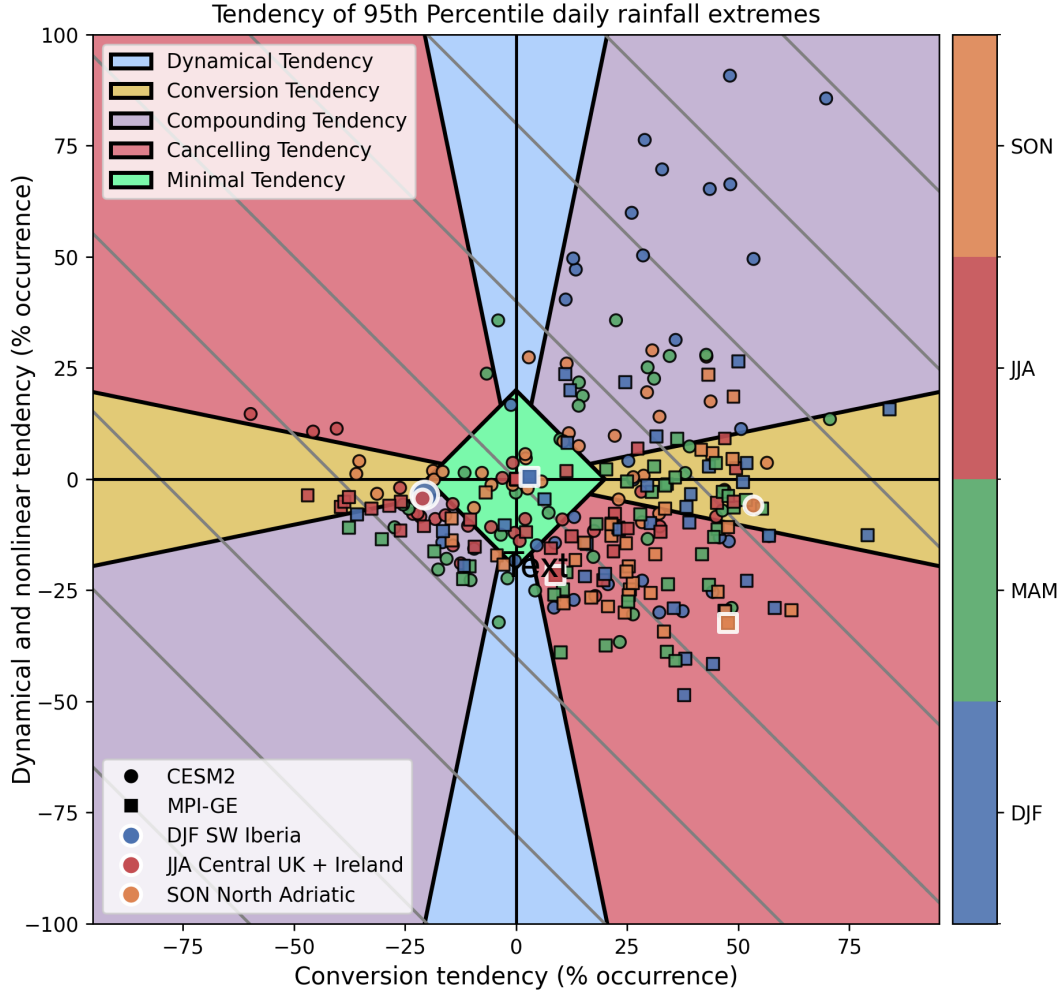


Figure 8: Heavy precipitation tendencies visualised in a tendency space as described in the main text. Ensemble mean results are shown for every region-season excluding cases where the heavy precipitation threshold is below 2.5mm/day. The three cases discussed in the main text are distinguished with a white border

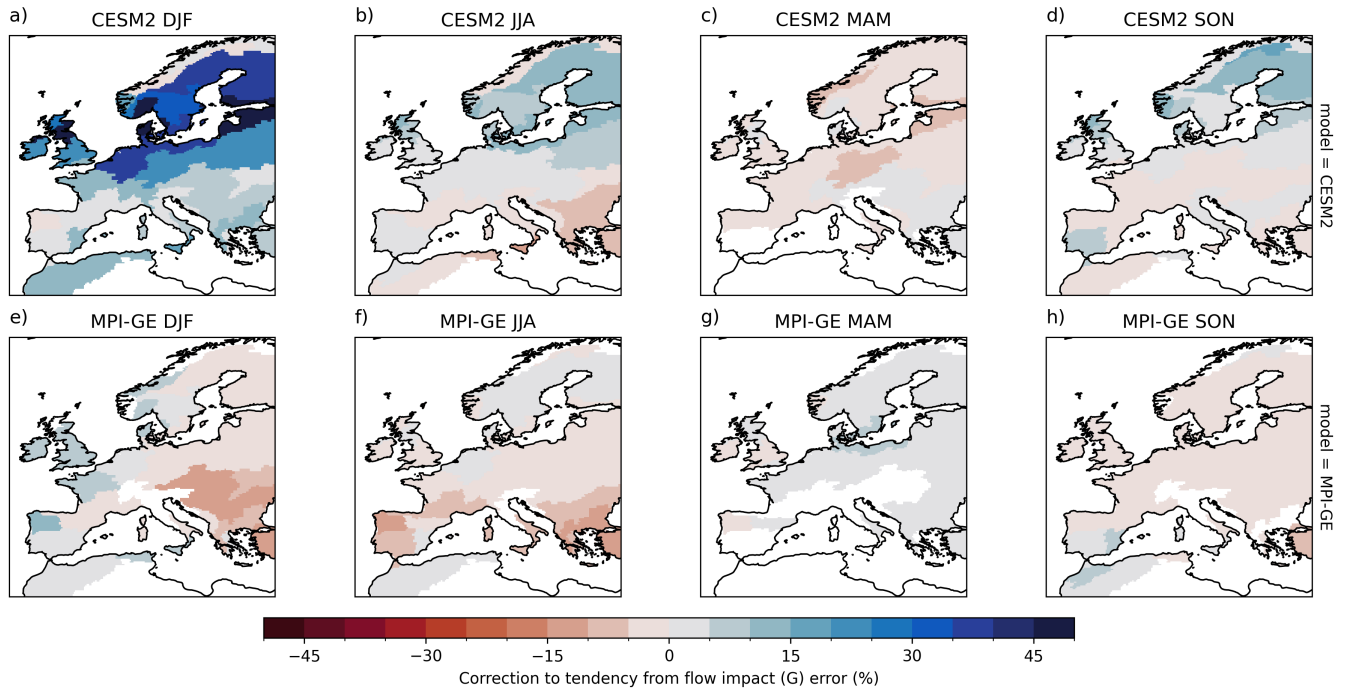


Figure 9: The flow-dependent correction to the relative precipitation tendency coming from model flow impact errors (term 2 in Equation 8 of the main text).

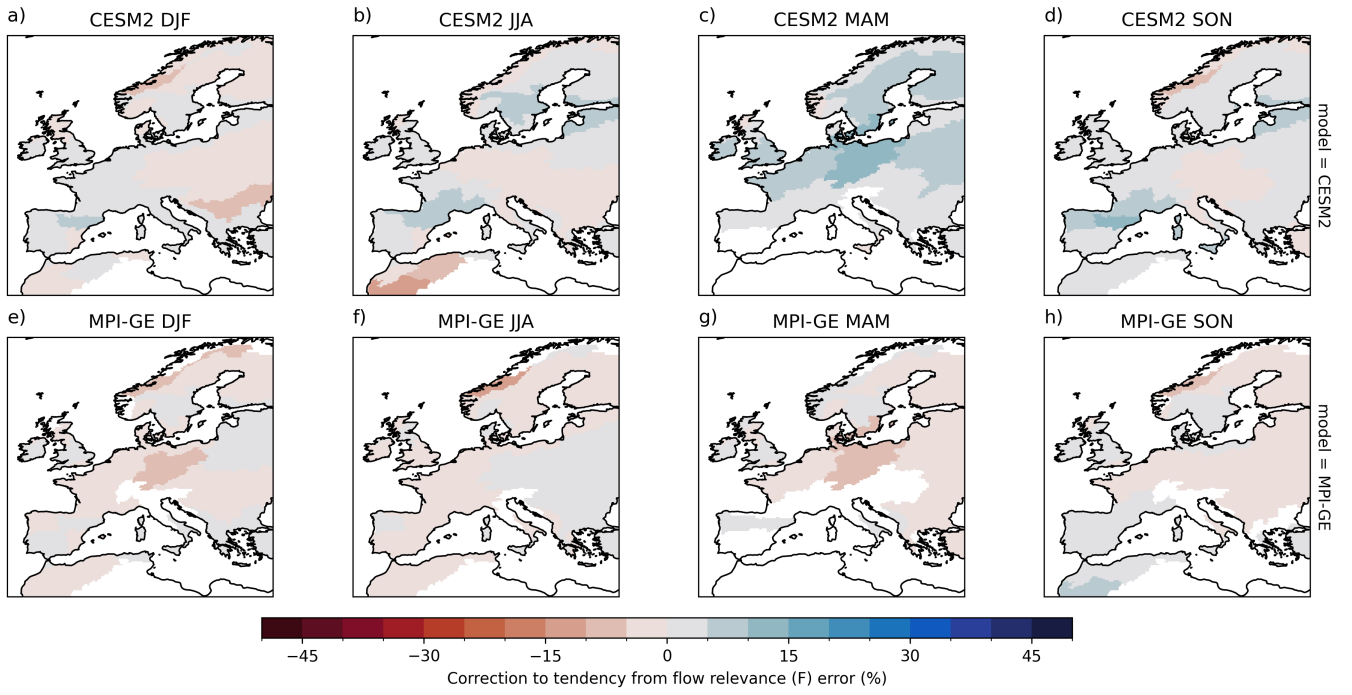


Figure 10: The flow-dependent correction to the relative precipitation tendency coming from model flow relevance errors (term 1 in Equation 8 of the main text).

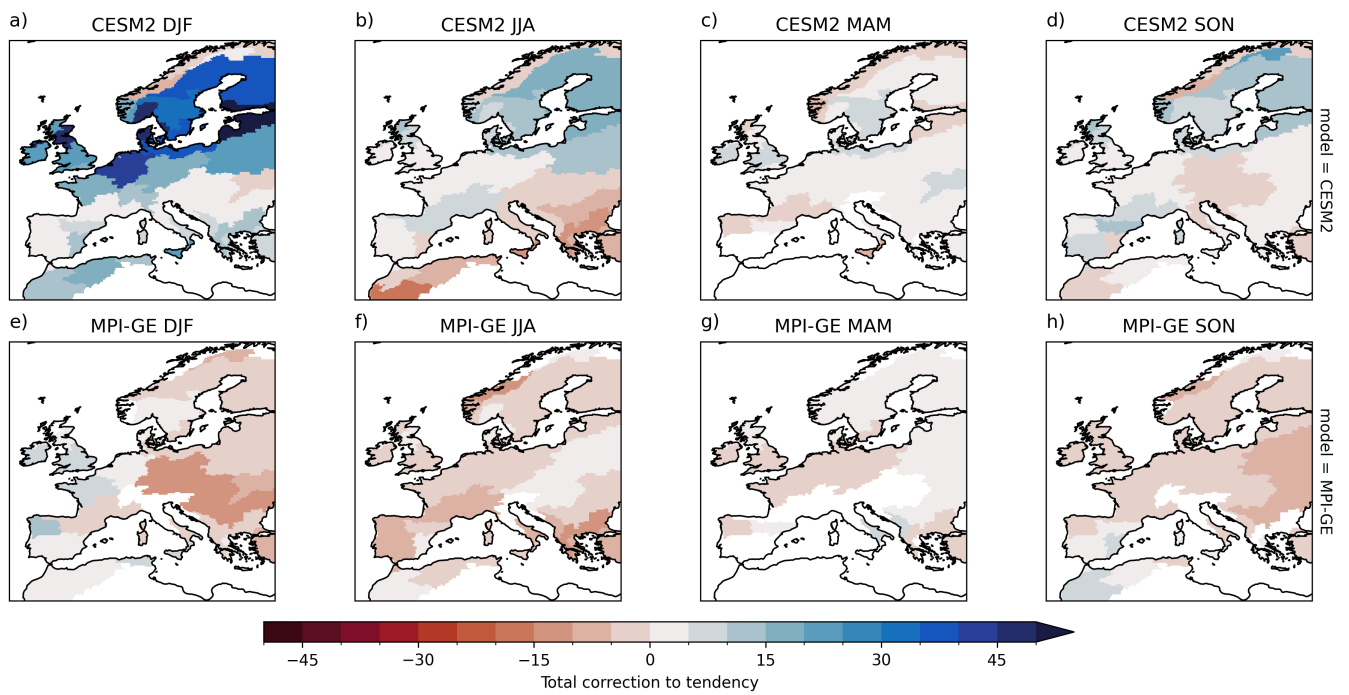


Figure 11: The total flow-dependent correction to the relative precipitation tendency ( $\tilde{\beta} - \beta$ ).